NEXAFS Depth Profiling of Surface Segregation in Block Copolymer Thin Films

ARTICLE *in* MACROMOLECULES · MAY 2010

Impact Factor: 5.8 · DOI: 10.1021/ma902866x

8 AUTHORS, INCLUDING:

Sitaraman Krishnan
Clarkson University
69 PUBLICATIONS **1,528** CITATIONS
SEE PROFILE

Christopher K Ober
Cornell University
587 PUBLICATIONS **15,869** CITATIONS
SEE PROFILE

NEXAFS Depth Profiling of Surface Segregation in Block-Copolymer Thin Films

Sitaraman Krishnan,[*,1] *Marvin Y. Paik,*[2] *Christopher K. Ober,*[2] *Elisa Martinelli,*[3] *Giancarlo Galli,*[3] *Karen E. Sohn,*[4] *Edward J. Kramer,*[5] *Daniel A. Fischer*[6]

[1] Clarkson University, Department of Chemical and Biomolecular Engineering, Potsdam, NY 13699;

[2] Department of Materials Science and Engineering, Cornell University, Ithaca, NY 14850;

[3] Dipartimento di Chimica e Chimica Industrial and UdR Pisa INSTM, Università di Pisa, 56126 Pisa, Italy;

[4] Department of Materials, University of California, Santa Barbara, CA 93106;

[5] Departments of Materials and Chemical Engineering, University of California, Santa Barbara, CA 93106;

[6] National Institute of Standards and Technology, Gaithersburg, MD 20899

* To whom correspondence should be addressed. E-mail: skrishna@clarkson.edu

Supporting Information

Dry films of the homopolymer, **H**, and the block copolymer, **C**, were analyzed using X-ray photoelectron spectroscopy. X-ray photoelectron spectroscopy (XPS) measurements were performed using a SSX-100 instrument (Surface Science Instruments, Inc.) with a monochromatized Al Kα X-ray source (1486.6 eV) operating in a vacuum of 1×10^{-9} Torr. The spectra were acquired at different electron emission angles, defined as the angle between electron-path toward the detector and the surface normal. Charge neutralization was carried out by injection of low energy electrons, and the C–C 1s peak was corrected to a binding energy of 285 eV.

Figure S1 shows a high resolution C1s XPS spectrum of the homopolymer film. The spectrum could be resolved into different sub-peaks as shown in the figure. Peak assignments were made based on the expected C 1s binding energies for different functional groups. The peak near 285 eV has contributions from the carbon atoms of styryl groups in the homopolymer. Note that it is difficult to resolve: the C–C carbon atoms from the $-CH_2-CH<$ repeat unit of the backbone; and C=C carbon atoms from the phenyl rings.

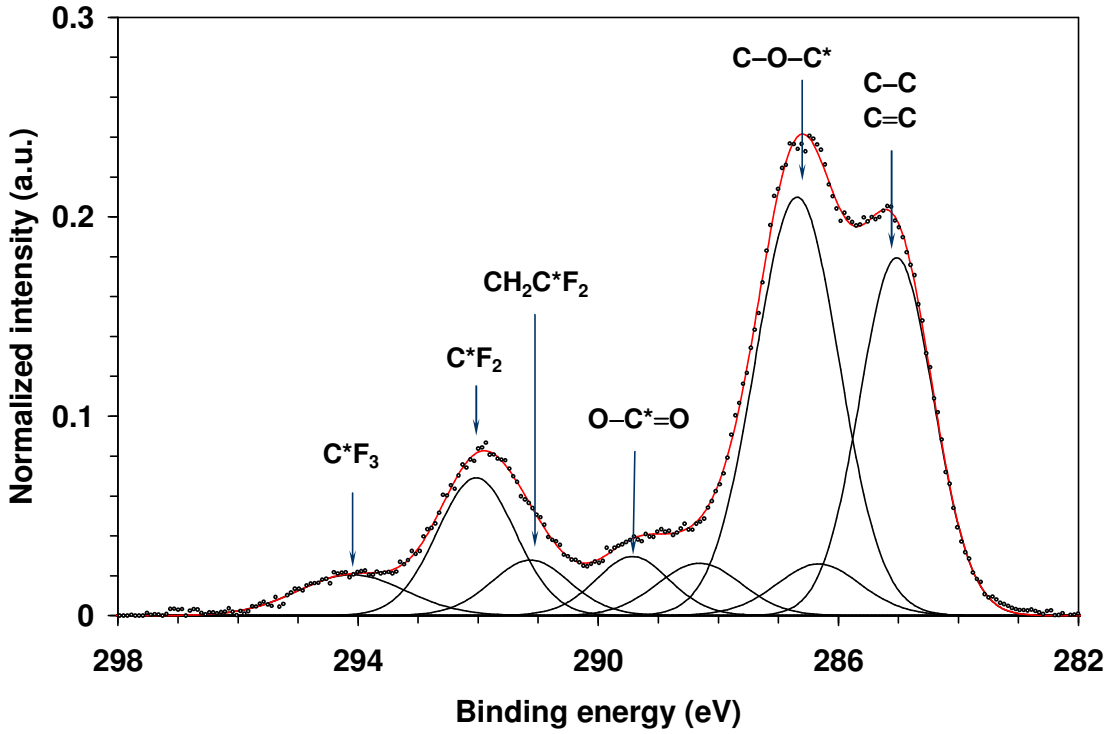

Figure S1. C 1s XPS spectrum of a dry surface of homopolymer **H**, acquired at an electron emission angle of 55° (with respect to the surface normal). Experimental data points are shown as dots, while fitted sub-peaks are shown by curves.

Angle dependent C 1s XPS spectra of 'dry' films of block copolymer **C,** consisting of cylindrical PS microdomains, is shown in Figure S2. Spectra acquired at three different emission angles, 0, 55, and 70°, are shown. It is fairly difficult to resolve the C=C peak and extract useful depth profiling information from these spectra. Such a surface could, however, be successfully analyzed for composition gradients using NEXAFS spectroscopy.

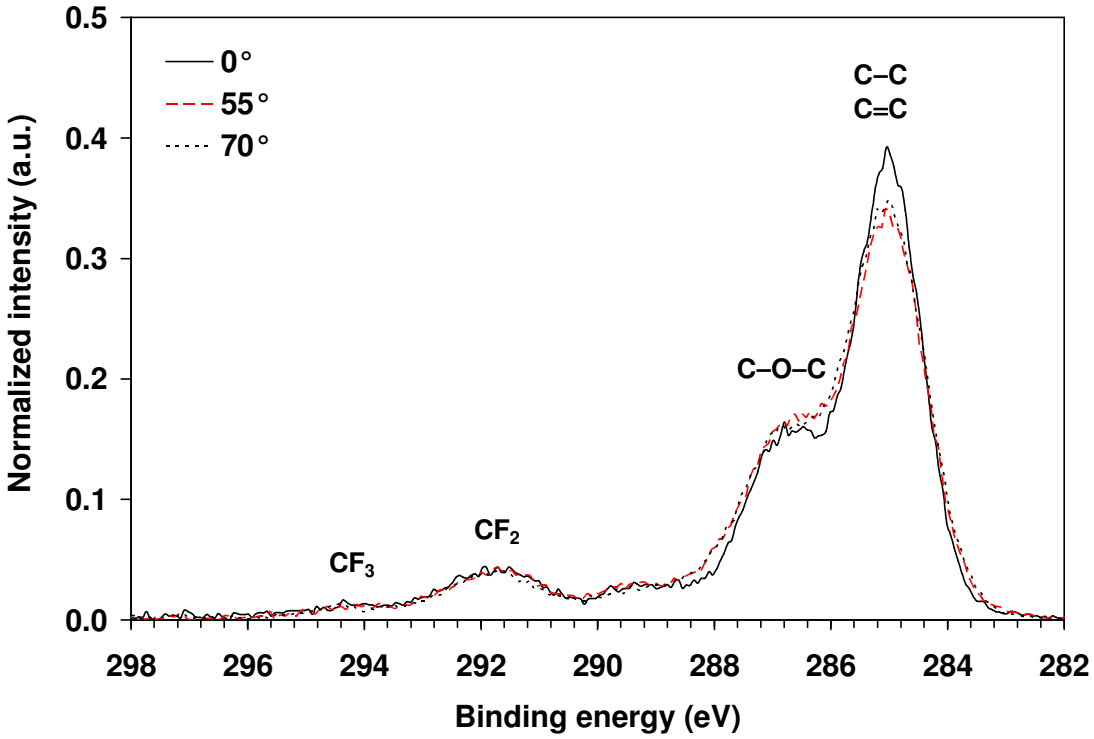

Figure S2. C 1s XPS spectra of a dry surface of block copolymer thin film that shows cylindrical microdomains. The cylinders lay parallel to the substrate. Spectra were acquired at electron emission angles of 0, 55 and 70°.

Surface Reconstruction During NEXAFS Data Acquisition. There was negligible surface reconstruction in the 'wet' surfaces when the samples were present in the NEXAFS chamber for data acquisition. Figure S3 shows NEXAFS spectra of the 'wet' block copolymer, **S**, with a spherical morphology acquired using 50° X-ray incidence. The two spectra were obtained at the same spot. The second spectrum, labeled 'repeat' was acquired 36 h after acquisition of the first spectrum. The sample remained in the NEXAFS chamber during this period, at room temperature. The differences in the two spectra are insignificant. A similar comparison using $\theta = 90°$, a more surface-sensitive analysis than 50° X-ray incidence, is shown in Figure S4. The spectra, which were acquired 36 h apart, are almost identical. Similar results were obtained for the random copolymer, **R** (Figure S5). Thus, the wet samples did not undergo surface reconstruction after removal from water, within the time scale of the NEXAFS data acquisition.

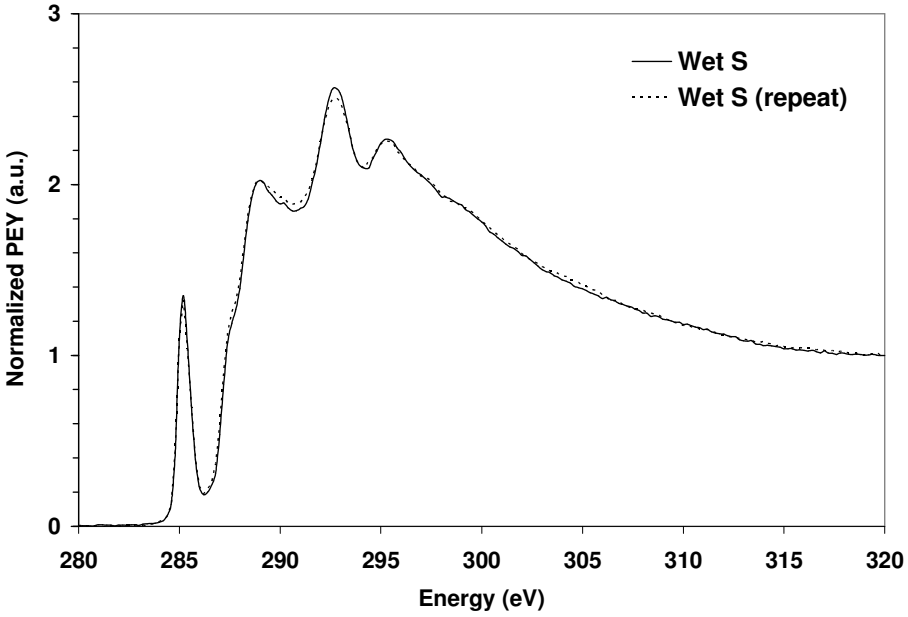

Figure S3. NEXAFS spectra of a 'wet' surface of block copolymer, **S**, acquired during time intervals that were 36 h apart; X-ray incidence angle = 50° and EGB = −150 V. The sample was kept at room temperature in an ultra-high vacuum environment of the NEXAFS chamber in between the two acquisitions.

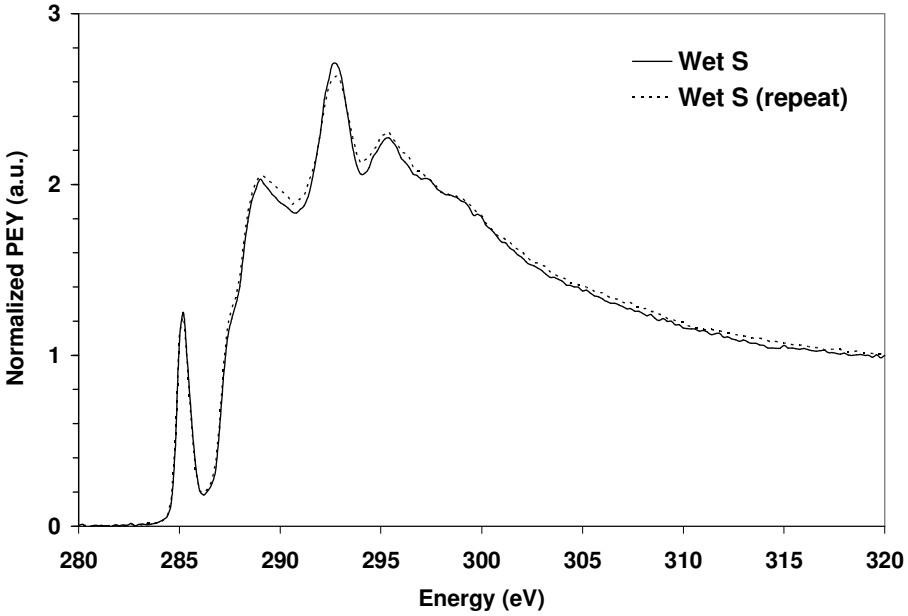

Figure S4. NEXAFS spectra of a 'wet' surface of block copolymer, **S**, acquired during time intervals that were 36 h apart; X-ray incidence angle = 90° and EGB = −150 V. The sample was kept at room temperature in an ultra-high vacuum environment of the NEXAFS chamber in between the two acquisitions.

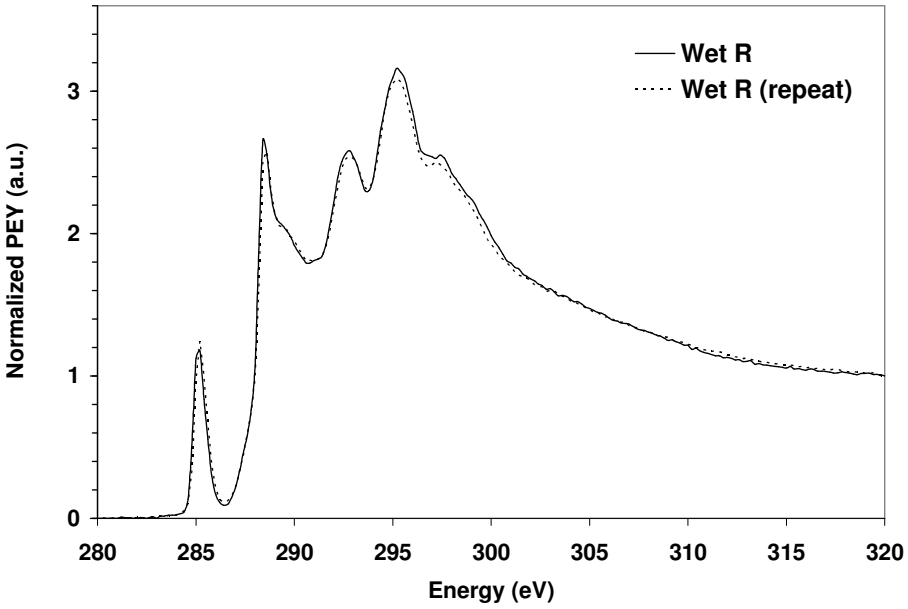

Figure S5. NEXAFS spectra of a 'wet' surface of random copolymer, **R**, acquired to confirm lack of surface reconstruction during NEXAFS data acquisition; X-ray incidence angle = 50° and EGB = −150 V.

Post-edge Normalized NEXAFS Spectra of Block Copolymer Films Acquired at Different X-ray Incidence Angles. Figure S6 shows the NEXAFS spectra of the 'dry' and 'wet' surfaces of block copolymer **C**, acquired at different X-ray incidence angles using an EGB = −150 V. While there are large variations in the $\pi^*_{C=C}$ peak intensity in NEXAFS spectra, angle resolved XPS of block copolymer **C** (cf. Figure S2) did not show similar sensitivity because of lack of sensitivity of XPS to C=C carbon atoms. The surface sensitivity of NEXAFS is higher than that of XPS. Using Al Kα X-ray, C 1s core shell photoelectrons with kinetic energy of about 1200 eV and hence an inelastic mean free path of about 3 nm are detected. The Auger electrons in C K-edge NEXAFS spectroscopy, on the other hand, have lower kinetic energies (~ 272 eV), and hence a lower inelastic mean free path (~ 1 nm). The lower inelastic mean free path of the Auger electrons leads to higher surface sensitivity in NEXAFS than XPS. The surface sensitivity is further improved in NEXAFS spectroscopy by applying a retarding potential at the entrance of the channeltron detector so that electrons from deeper in the sample that have lost more energy are not detected.

Figure S7 shows the normalized C 1s NEXAFS spectra of the dry and wet surfaces of block copolymer **S**, acquired at different X-ray incidence angles. As in the case of block copolymer **C**, the $\pi^*_{C=C}$, $\pi^*_{C=O}$, and σ^*_{C-F} resonance intensities of 'dry' and 'wet' films of block copolymer **S** varied significantly with the angle of X-ray incidence suggesting a non-uniform concentration profile near the surfaces. It is clearly seen that the intensities of $\pi^*_{C=C}$ resonances (denoted by +) and the σ^*_{C-F} resonances (denoted by *) show opposite trends in their dependence on the X-ray incidence angle.

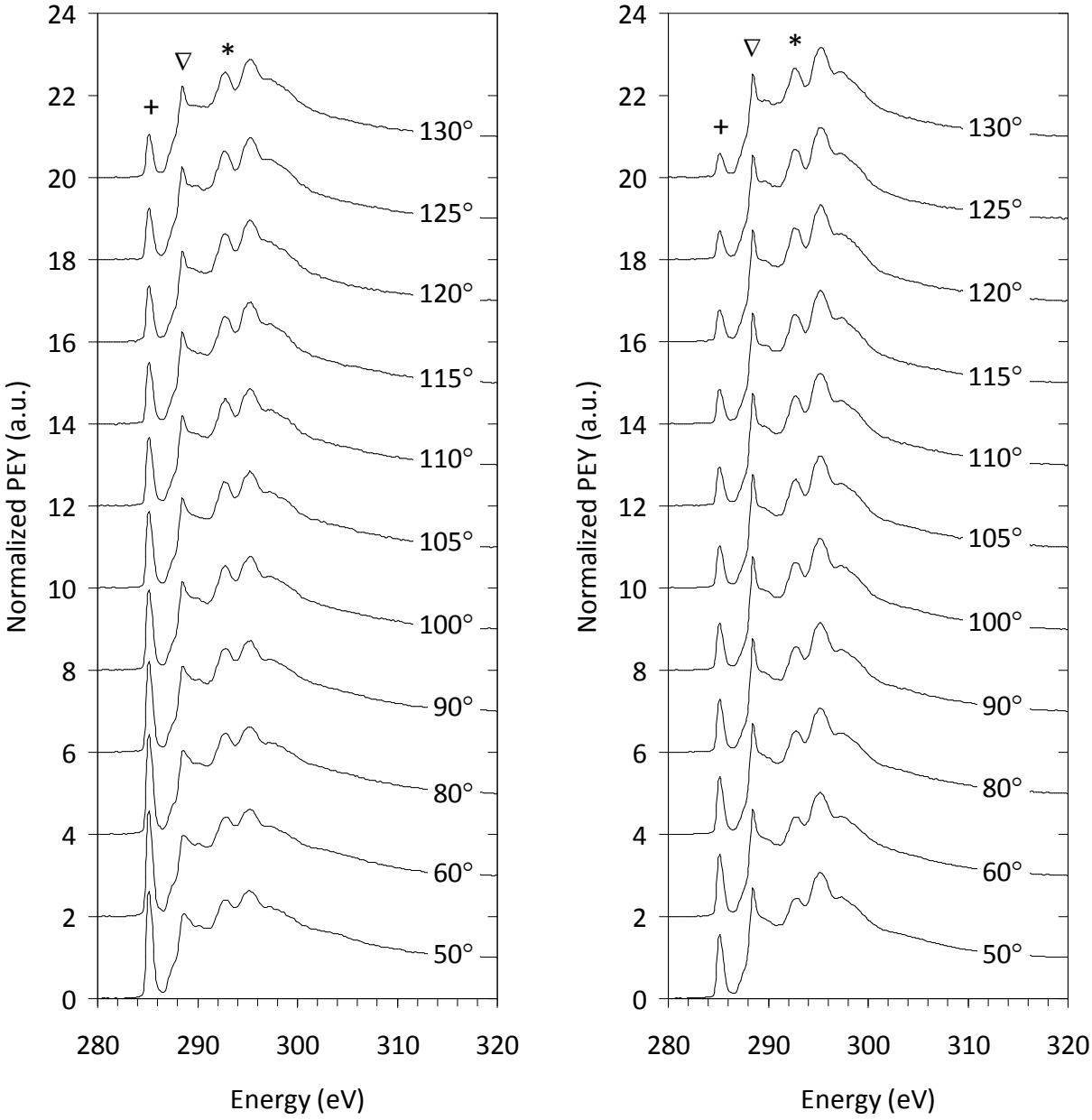

Figure S6. Post-edge normalized C 1s NEXAFS spectra of 'dry' (left) and 'wet' (right) thin films of block copolymer **C** with cylindrical PS microdomains; EGB = −150 V. Note the variation in the intensities of the peaks corresponding to $\pi^*_{C=C}$, $\pi^*_{C=O}$, and σ^*_{C-F}, marked as +, ∇, and *, respectively.

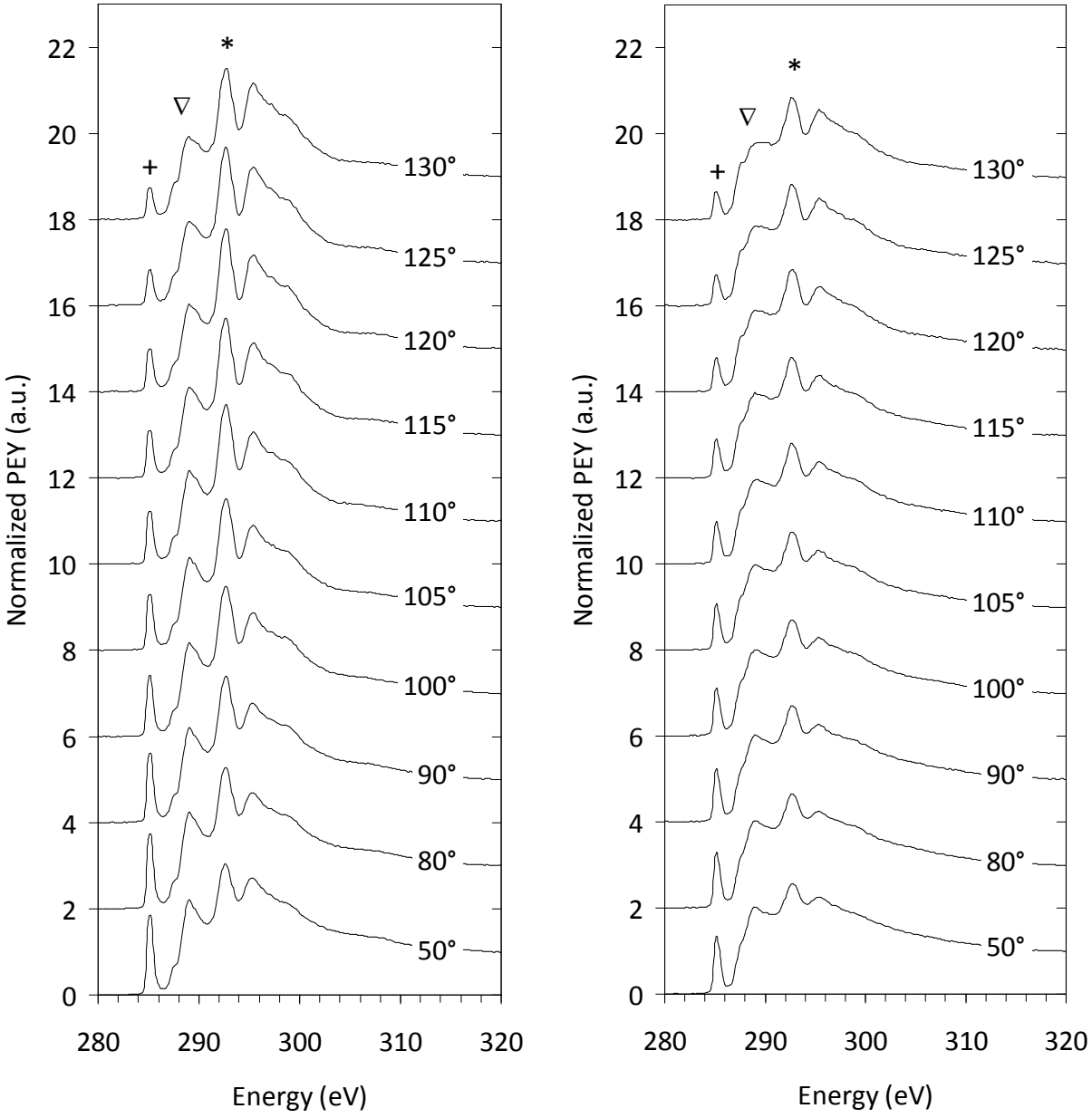

Figure S7. C 1s NEXAFS spectra of 'dry' (left) and 'wet' (right) thin films of block copolymer **S** with spherical PS microdomains; EGB = −150 V. Note the variation in the intensities of the peaks corresponding to $\pi^*_{C=C}$, $\pi^*_{C=O}$, and σ^*_{C-F}, marked as +, ∇, and *, respectively.

Compositional Depth-Profiling Using NEXAFS. The following empirical equation with three adjustable parameters that can be used to produce surface or bulk layers of different compositions, and an adjustable gradient between them, was used to model the number fraction of phenyl ring carbon atoms as a function of depth, z/λ, below the surface.

$$f_{C=C} = \frac{f_\infty}{1 + \mathrm{e}^{-\frac{1}{\xi}\left(\frac{z}{\lambda} - \beta\right)}} \tag{S1}$$

The parameters ξ and β characterize the steepness and position of the inflection point of the sigmoidal concentration profile. The equation relating post-edge normalized intensity, I_a, of an Auger peak to the X-ray incidence angle, θ, and electron emission angle φ is given by:

$$I_a = \frac{A}{\lambda \cos\varphi}\left\{\frac{1}{3} + \left(P\cos^2\theta - \frac{1}{3}\right)S\right\}\int_0^\infty f_i(z)\exp\left\{-\frac{z}{\lambda\cos\varphi}\right\}\mathrm{d}z \tag{S2}$$

where λ is the electron escape depth, S is the bond orientational order parameter, and P is the degree of polarization of the X-ray beam. The substitution of $f_i(z)$ in eq S2 with the expression for $f_{C=C}$ in eq S1 resulted in a non-linear equation with four parameters, Af_∞, ξ, β and S, which after a change of variable could be written in a form suitable for data fitting:

$$I_a = \frac{Af_\infty}{3} \times \left\{1 + \left(3P\cos^2\theta - 1\right)S\right\} \times \int_0^1 \frac{1}{1 + \exp\left\{\left(\beta + \cos\varphi \cdot \ln x\right)/\xi\right\}}\mathrm{d}x \tag{S3}$$

The unknown parameters were determined for each surface from the experimental data of normalized Auger electron intensity, I_a, versus the X-ray incidence angle, θ. Note that the X-ray emission angle, φ, is equal to $\left(\theta + \Delta - 90^\circ\right)$ (cf. Figure 2 in the paper), and is not independent of θ.

When the incidence angle, θ, is equal to 51.2° or 128.8°, $P\cos^2\theta - \frac{1}{3} = 0$. Thus, at the magic angle, θ^* ≈ 51.2° or 128.8°, the normalized Auger electron intensity, I_a^*, is given by:

$$I_a^* = \frac{Af_\infty}{3} \times \int_0^1 \frac{1}{1 + \exp\left\{\left(\beta + \cos\varphi^* \cdot \ln x\right)/\xi\right\}}\mathrm{d}x \tag{S4}$$

where φ^* is the emission angle corresponding to the magic angle θ^*. Determination of numerical values of the parameters Af_∞, ξ, β and S is aided by the fact that eqs S3 and S4 can be combined to eliminate the product Af_∞:

$$\frac{I_a}{I_a^*} = \left\{1 + \left(3P\cos^2\theta - 1\right)S\right\} \times \frac{\displaystyle\int_0^1 \frac{1}{1 + \exp\left\{\left(\beta + \cos\varphi \cdot \ln x\right)/\xi\right\}}\mathrm{d}x}{\displaystyle\int_0^1 \frac{1}{1 + \exp\left\{\left(\beta + \cos\varphi^* \cdot \ln x\right)/\xi\right\}}\mathrm{d}x} \tag{S5}$$

In eq S5, I_a is the normalized PEY (peak height) of the C 1s → $\pi^*_{C=C}$ resonance at X-ray incidence angle θ, and I_a^* is the normalized PEY at the X-ray incidence angle $\theta = 50°$ (which is close to the magic angle of 51.2°). The values of S, β and ξ were estimated from the I_a / I_a^* vs. θ data using the non-linear least squares curve fitting technique. S was constrained between 1 (where the phenyl ring π orbitals are oriented normal to the surface) and –0.5 (where the π orbitals are oriented parallel to the surface). The best-fit values of the parameters, ξ, β, S, and the product Af_∞, were then determined using eq S3.

Parameter A characterizes the ratio of, $\sigma_{x,i}$, the X-ray absorption cross section of the phenyl ring carbon atoms at resonance (corresponding to the C 1s $\rightarrow$ $\pi^*_{C=C}$ transition at 285.2 eV) to, $\sigma_x\big|_{320\ eV}$, the X-ray absorption cross section at a photon energy far from resonance (at 320 eV). There are two types of phenyl rings in the copolymer samples, namely, the phenyl rings in the PS block, Φ, and the phenyl rings in the PEGylated/fluorinated block, Φ–COOR. However, the $\sigma_{x,i}$ values for Φ and Φ–COOR are fairly close because neither of the phenyl rings contain electronegative atoms (in contrast to, for example, poly(4-vinyl pyridine), where one carbon atom in the phenyl ring is replaced by a nitrogen atom), and an ester group is only moderately electron-withdrawing (unlike a nitro or amino group where the phenyl ring is directly attached to an atom that is more electronegative than carbon). Indeed, the value of $A = 23 \pm 2$ calculated using the I_a vs. θ values for homopolymer **H,** was found to be in reasonable agreement with the value determined from the I_a vs. θ data for a PS homopolymer thin film ($A \cong 22$). Finally, knowing A, the value of f_∞ could be calculated, for the PEGylated/fluorinated surfaces investigated in this study, from the Af_∞ values obtained by data fitting.

Physical Significance of f_∞. According to eq S1, f_∞ is the fraction of the total number of carbon atoms that belong to the phenyl rings, far from the surface $\left(z/\lambda \rightarrow \infty\right)$. However, for $z/\lambda > 3$, regardless of the value of $f_{C=C}$, the integrand in eq S2 is close to 0, especially at higher emission angles ($\cos\varphi \rightarrow 0$). The Auger electrons emitted below depths of $z/\lambda = 3$ have negligible contribution to the experimentally determined partial electron yield so that this region is essentially not probed. In general, therefore, the value of f_∞, obtained by fitting eq S3 to I_a vs. θ need not be equal to the actual number fraction of phenyl ring carbon atoms in the 'bulk', which we denote by f_b. NEXAFS does not probe the bulk of the film. The NEXAFS probe-depth is limited to $z/\lambda = 3$.

Table S1 gives the values of the parameters of the depth profile model (eq S1) for the six copolymer surfaces, determined using the experimental I_a vs. θ data.

Table S1. Parameters of the concentration profile model in eq 11, representing depth profiles of dry and water-immersed surfaces of styrenic polymers with PEGylated fluoroalkyl groups.

Surface	Af_∞	S	ξ	β	f_∞ [(a)]	f_{avg} [(b)]
Dry **C**	21.4	0.013	0.582	1.019	0.93	0.37
Wet **C**	14.4	0.017	0.599	1.482	0.63	0.22
Dry **S**	15.3	–0.003	0.571	1.309	0.66	0.26
Wet **S**	10.7	–0.041	0.761	1.445	0.47	0.17
Dry **R**	11.9	–0.022	0.476	0.948	0.52	0.27
Wet **R**	7.9	–0.070	0.616	1.046	0.34	0.17

[(a)] calculated from Af_∞ using $A = 23$

[(b)] average of $f_{C=C}$ over the range $z/\lambda = 0$ to $z/\lambda = 2$

A Simpler Depth Profile Model with More Adjustable Parameters. In Table S1, the values of the orientational order parameter S are close to 0, indicating that the phenyl rings are not oriented at the surface. The assumption of $S = 0$, and the use of linear concentration profiles, allowed analytical determination of the parameters of the concentration profile using eq S2. The resulting concentration profiles are shown in Figure S8. These concentration profiles are in good agreement with results obtained using the model in eq S1. They also resulted in a satisfactory fit of the I_a vs. θ data.

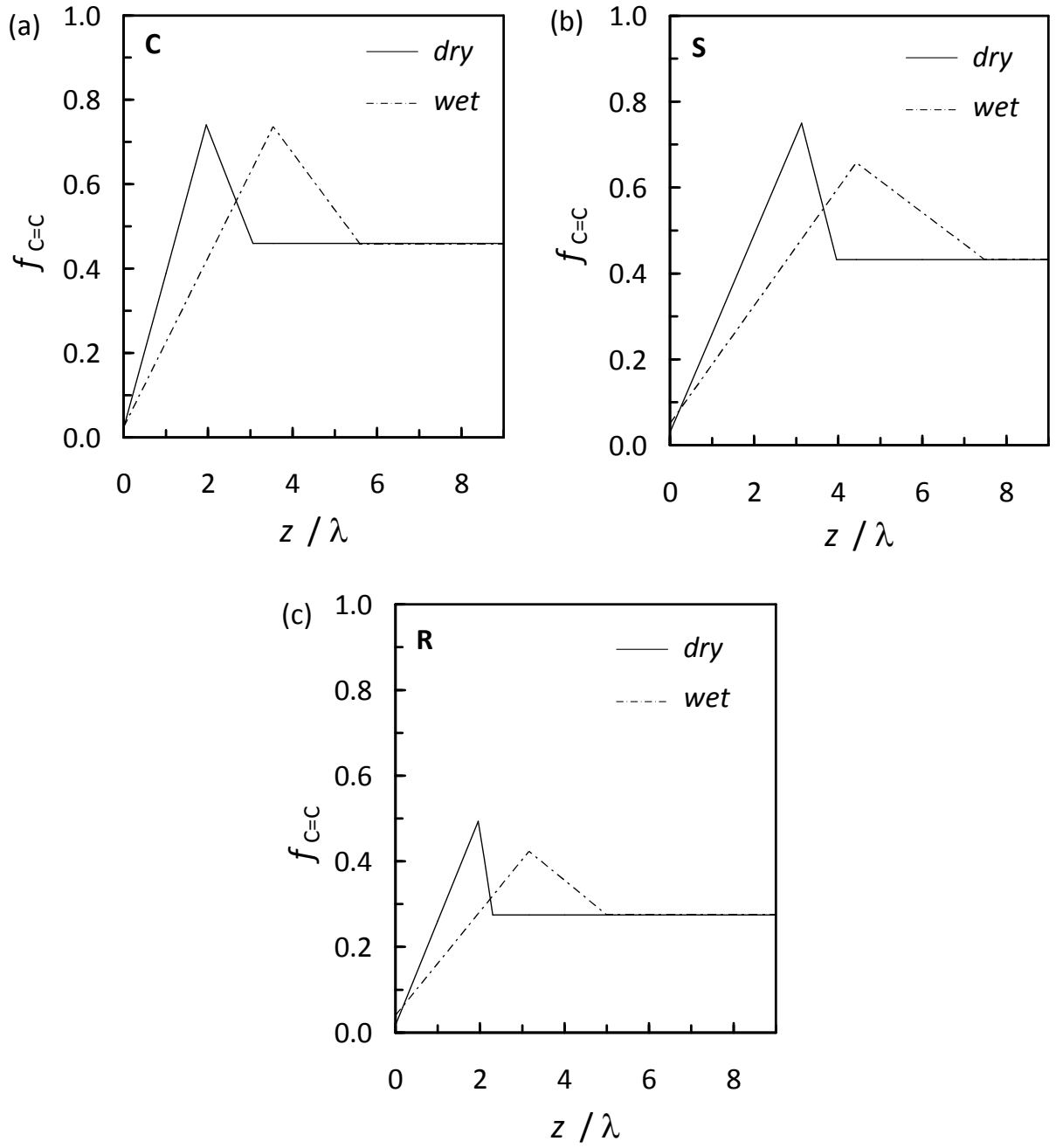

Figure S8. (a–c) Concentration depth profiles in 'dry' and 'wet' thin films of copolymers **C** (a), **S** (b), and **R** (c).

Assumption of Depth-invariant Number Density of Carbon Atoms in the Film. We have assumed that $\sum_i \rho_i(z)$ is constant throughout the polymer film, and is independent of depth. ρ_i (atoms/cm^3) is the number concentration of carbon atoms involved in a chemical bond of type *i*, and $\sum_i \rho_i$ is the total number of carbon atoms per unit volume of polymer. The average number density of carbon atoms in a polymer can be calculated using:

$$\sum_i \rho_i = \frac{\rho_P N_A n_C}{M_0} \qquad \text{(S6)}$$

where ρ_P (g/cm^3) is the polymer density, M_0 (g/mol) is the monomer molecular weight, N_A is Avogadro's number (no. per mol), and n_C is the number of carbon atoms per monomer. Thus, the number density of carbon atoms is about is 49 nm^{-3} in polystyrene, and about 35 nm^{-3} averaged over the entire homopolymer **H.** The fluorocarbon portion of the side chains would have a carbon atom density of 24 nm^{-3}, and the –$(CH_2CH_2O)_xCH_2CH_2(CF_2CF_2)_yF$ side chain, a carbon atom density of 27 nm^{-3}. Although the depth profiles derived show a significantly increased side chain fraction (decreased $f_{C=C}$) near the surface and thus for consistency the $\sum_i \rho_i(z)$ cannot be constant as a function of depth, this complication is ignored to simplify the analysis.

Polymer molecular weight distributions. Figure S9 shows the size exclusion chromatography chromatograms of homopolymer **H**, which was synthesized using 2,2′-azobisisobutyronitrile by conventional free radical polymerization, the PS macroinitiator that was synthesized by atom transfer radical polymerization (ATRP), and block copolymer **C**, also synthesized by ATRP. As expected, the PS macroinitiator and the block copolymer, which were prepared by controlled radical polymerization, had narrower molecular weight distributions than homopolymer **H** that was prepared using conventional free radical polymerization. The unimodal distribution, and relative peak positions in the chromatograms for the macroinitiator and the block copolymer, clearly show successful formation of a block copolymer by addition of the PEGylated/fluorinated monomer to the PS macroinitiator.

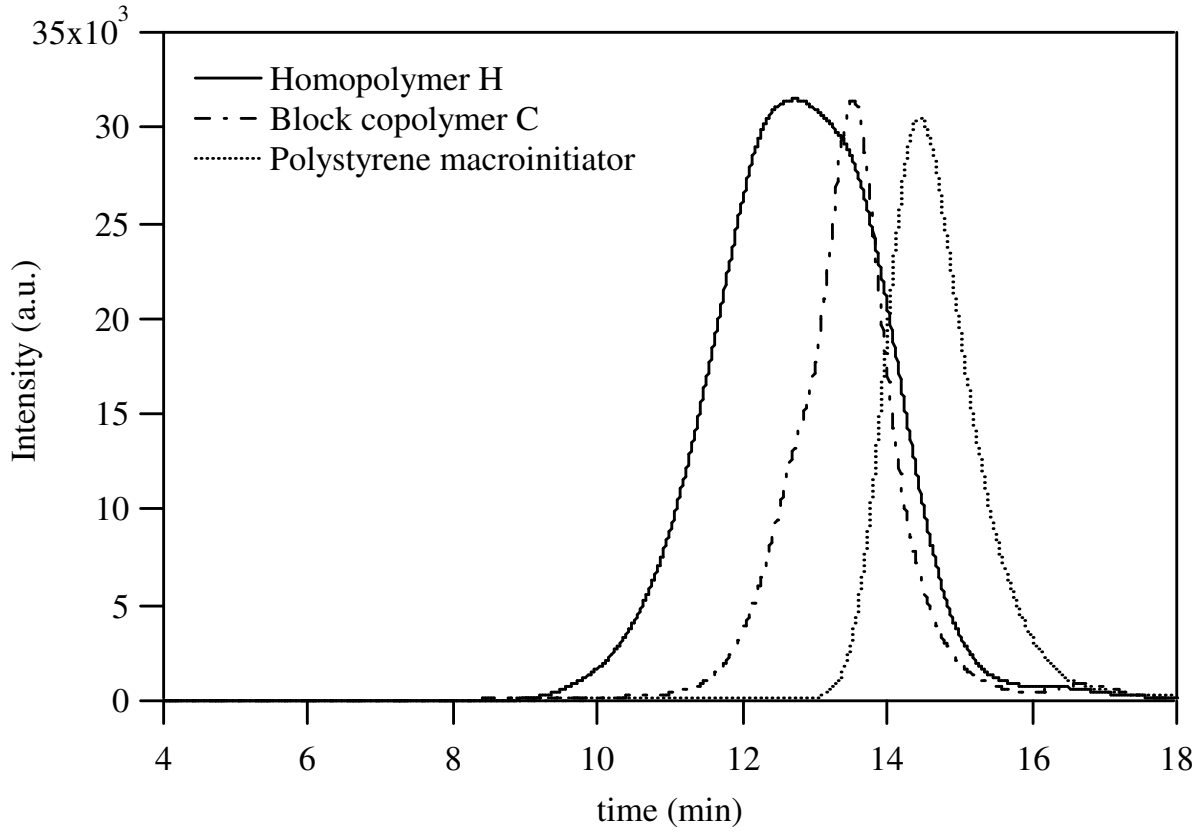

Figure S9. GPC chromatograms of PS macroinitiator (·····) and block copolymer **C** (– · – ·), and homopolymer **H** (———).